J Mater Sci: Mater Med (2008) 19:167–173
DOI 10.1007/s10856-006-0056-3

Preparation, mechanical properties and in vitro degradability of wollastonite/tricalcium phosphate macroporous scaffolds from nanocomposite powders

Faming Zhang · Jiang Chang · Kaili Lin · Jianxi Lu

Received: 19 January 2006 / Accepted: 27 November 2006 / Published online: 28 June 2007
© Springer Science+Business Media, LLC 2007

Abstract A new class of scaffolds with a gain size of 200 nm was prepared from wollastonite/tricalcium phosphate (WT) nanocomposite powders (termed ''nano-sintered scaffolds'') through a two-step chemical precipitation and porogen burnout techniques. For a comparison, WT scaffolds with a grain size of 2 μm were also fabricated from submicron composite powders (termed ''submicron-sintered scaffolds'') under the same condition. The resultant scaffolds showed porosities between 50 ± 1.0% and 65 ± 1.0% with a pore size ranging from 100 μm to 300 μm. The WT nano-sintered scaffolds exhibited compressive strength and elastic modulus values that were about twice that of their submicron-sintered counterparts. The in vitro degradation tests demonstrated that the degradability could be regulated by the grain size of bioceramics. The decreased specific surface area of pores in the nano-sintered scaffolds led to their reduced degradation rate. The mechanical properties of the nano-sintered scaffolds exhibited less strength loss during the degradation process. The WT macroporous nano-sintered scaffolds are a promising and potential candidate for bone reconstruction applications.

F. Zhang · J. Chang (✉) · K. Lin · J. Lu
Biomaterials and Tissue Engineering Research Center, Shanghai Institute of Ceramics, Chinese Academy of Sciences, Shanghai 200050, China
e-mail: jchang@mail.sic.ac.cn

J. Lu
Institut de Recherche sur les Biomatérieux et les Biotechnologies, Université du Littoral Côte d'Opale, Berck sur Mer Cedex 62608, France

Introduction

Bone defects that occur due to surgery, trauma, or abnormal development require skeletal reconstruction. Bone reconstructive methods require grafts or synthetic material to replace lost bone or enhance new bone formation [1]. Since their compositions are similar to the inorganic components of bone, calcium phosphate bioceramics, especially hydroxyapatite (HA) and β-tricalcium phosphate (β-TCP), have been extensively explored as grafts for bone regeneration applications [2]. HA possesses excellent bioactivity whereas β-TCP exhibits biodegradability. Therefore, many studies have focused on developing HA/β-TCP biphasic calcium phosphate (BCP) bioceramics because their biological performances are more effective than pure HA or β-TCP [3–5]. The bioactivity and biodegradability of BCP composites could be controlled by modulating the HA/β-TCP ratio.

Recent studies revealed that wollastonite ($CaSiO_3$) ceramics are bioactive and can be used as a new bioactive material [6, 7]. Recent studies in our group showed that the wollastonite ceramics also possess better mechanical properties and more degradability than HA [8–11]. It is well known that the HA ceramics are brittle and almost not degradable. Expectedly, the mechanical properties of the grafts could be enhanced by using wollastonite instead of HA with β-TCP phase. De Aza et al. first studied the wollastonite/TCP (WT) composite and found it has good bioactivity as evidenced by deposition of a bone like apatite layer on the surface of the composite [12]. Huang et al. investigated the apatite formation mechanism on wollastonite/β-TCP surfaces [13]. The above studies mainly focused on the bioactivity of the dense WT bioceramics without consideration of the mechanical properties and degradability. Although the dense WT bioceramics could

develop in situ microporous structure after being soaked in simulated body fluid (SBF) [12, 13], bioceramics scaffolds with a three-dimensional (3D) macroporous structure are preferred to improve new bone ingrowth and facilitate tissue regeneration. It is proved that pores with a diameter between 50 μm and 150 μm can stimulate osteoid formation, and those in the range of 150–500 μm can lead to the formation of mineralized bone directly [11]. However, there are many challenges in developing macroporous bioceramics scaffolds. The major challenge is their poor mechanical properties since increased porosity generally leads to decreased strength [14]. Recently, the concept of nanocomposites has been introduced to porous scaffolds and the mechanical properties have been significantly improved in BCP nanocomposite scaffolds [5]. The objectives of the present work are to prepare WT macroporous scaffolds from nanocomposite powders (termed ''nano-sintered scaffolds''), to assess the microstructure, mechanical properties, in vitro degradability of the prepared scaffolds in comparison with the submicron composite powders sintered counterparts (termed '' submicron-sintered scaffolds'') processed under the same conditions.

Materials and methods

Powder synthesis

The WT nanocrystalline composite powders with a weight ratio of 5/5 were prepared by a two-step chemical precipitation method. A 0.2 M Ca $(NO_3)_2$ solution with a pH of 11.5 was stirred at room temperature and 0.2 M Na_2SiO_3 was added to it drop wise at a rate of 1.5 mL/min to produce white precipitates. Then, the produced precipitates were stirred for another 24 h followed by washing with NH_4OH and ethanol, and drying at 80 °C for 24 h. The powders were calcined at 700 °C for 2 h to obtain amorphous calcium silicate ($CaSiO_3$) powders, which were then dispersed into 0.2 M $(NH_4)_2HPO_4$ solution, and 0.2 M $Ca(NO_3)_2$ was added drop-wise to produce white precipitates. The pH of the solution was adjusted to 10.8 using NH_4OH. After being stirred and washed, the white precipitates were dried at 80 °C for 24 h. Finally, the synthesized nanocomposite powders were calcined at 800 °C for 2 h. In addition, some composite powders were also calcined at 1050 °C for 5 h to get a much coarser particle size for a comparison.

Scaffolds preparation

The obtained WT powders were sieved and mechanically mixed with polyethylene glycol (PEG) particulates with a size of 150–350 μm. The mixtures with 10.0 wt.% polyvinyl alcohol (PVA) were pressed at 8 MPa uniaxially in a stainless steel die. The porosity of the substrate was adjusted by varying the amount of PEG. The green disks with a diameter of 10 mm and a thickness of 8 mm were heat-treated at 400 °C for 2 h to remove the organic substances, and then they were pressureless sintered at 1100 °C and 1130 °C for 5 h at a heating rate of 1 °C/min, and then furnace-cooled to the room temperature.

Structures and properties analysis

The morphologies of the calcinated WT composite powders were observed by scanning electron microscopy (SEM, JSM-6700F, Japan). X-ray diffraction (XRD, Rigaku D/max 2550V, Japan) with Cu$K\alpha$ radiation was used to characterize the phase composition of the powders and ceramics. Porosity of the sintered samples was determined by the Archimedes method. Quantachrome porosimeter (PoreMaster 33) was employed to measure the microporosity of the scaffolds. The compressive strength was conducted on a mechanical tester with a 0.5 mm/min crosshead speed (AG-5KN, Shimadza, Japan). The elastic modulus was reanalyzed from the slope of the compressive strength–strain curve. For mechanical strength and porosity, five samples of each group were used for statistical analysis. Moreover, SEM analysis of the fractured surfaces of the bioceramic samples was performed on an electron microprobe analyzer (EPMA, 8705QH_2, Japan).

The in vitro degradability of the macroporous WT composite bioceramics was determined by their weight loss percentage in a Tris–HCl buffer solution. The Tris–HCl solution was prepared by dissolving tris-hydroxymethyl aminomethane (analytical reagent grade) in distilled water with buffering at pH 7.4 ± 0.1 by 0.1 mol/L hydrochloric acid at 37.0 °C. The porous WT composites were suspended in polystyrene bottles containing Tris–HCl solution at 37.0 °C in a shaking water bath. The ratio of surface area (cm^2) to solution volume (mL) was 1/10. The soaking solution was refreshed every 24 h. Three samples of each group were collected after 1, 3, 5, 7, 14 and 21 days soaking, respectively. At each time point, the samples were taken out, rinsed with deionized water, and dried in an oven at 150 °C for 48 h. Finally, the weight loss and compressive strength loss of the scaffolds were measured.

Results and discussion

Powder characterization

The WT nanocrystalline composite powders were prepared using a chemical precipitation process via a two-step chemical reaction:

$$Ca(NO_3)_2 + Na_2SiO_3 \rightarrow CaSiO_3 + 2NaNO_3 \quad (1)$$

$$3Ca(NO_3)_2 + 2(NH_4)_2HPO_4 + 2NH_4OH \rightarrow Ca_3(PO_4)_2 + 6NH_4NO_3 + 2H_2O \quad (2)$$

In the first step, amorphous calcium silicate was obtained, and then was dispersed into the second step reaction solution. Finally, the composites comprised of $CaSiO_3$ and $Ca_3(PO_4)_2$ were precipitated together. The SEM image of the precipitated WT composite powders calcined at 800 °C is given in Fig. 1a. The powders exhibit a rod-like shape and a uniform particle size (30 nm in diameter and 100 nm in length). On the contrary, the powders calcined at the higher temperature (1050 °C) are much coarser have a particle size on a submicron scale as noted in Fig. 1b. The particles calcined at higher temperature agglomerated together and the average particle size was 200 nm in diameter and 500 nm in length. No phases other than β-$CaSiO_3$ and β-TCP were revealed in the calcined composite powders by X-ray diffraction analysis (Fig. 2). The β-$CaSiO_3$ powders that calcined at 1050 °C were not transformed into the α form.

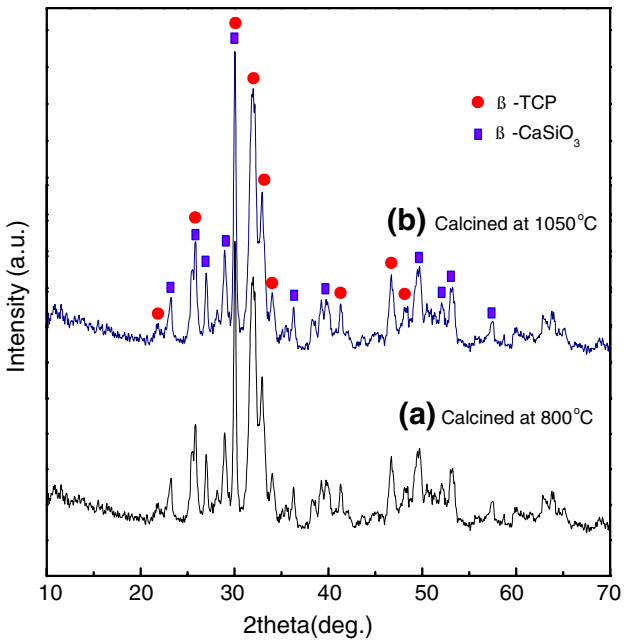

Fig. 2 X-ray diffraction patterns of the calcined WT composite powders

Microstructures and mechanical properties

The two types of powders were mixed with different weight percentages of PEG particulates. After sintering and porosity characterization by Archimedes methods, it was found that much more PEG particulates were needed to obtain the same porosity in the nano-sintered scaffolds. The porosity of the nano-sintered scaffolds with 50 wt. % PEG porogen addition is 55 vol.%. However, the submicron-sintered scaffolds with the same PEG content had measured porosity up to 65 vol.%. Microporosity is defined by a pore size <10 μm [15]. Microporosity in the sintered porous WT scaffolds have been measured and calculated statistically. The microporosity of nano-sintered scaffolds (30 vol.%) is lower than that of the submicron-sintered scaffolds (38 vol.%). Microporosity is a result of sintering process where the original particle size, sintering temperature and time are critical parameters. The porogen additions have little effect on the microporosity. The lower microporosity of the nano-sintered scaffolds resulted in a higher density of the scaffolds. Accordingly, such differences between the two scaffolds could be attributed to the finer particle size, higher shrinkage rate and density of the nano-sintered scaffolds.

Figure 3 shows the X-ray diffraction patterns of the WT nano-sintered scaffolds at temperature of 1100 °C and 1130 °C. The β-$CaSiO_3$ has transformed into their high temperature phase α-$CaSiO_3$ after sintering at 1130 °C while the β-TCP remains stable. Our previous study on the β-$CaSiO_3$ dense ceramics showed that the β-$CaSiO_3$ changed into α-$CaSiO_3$ at 970 °C in spark plasma sintering

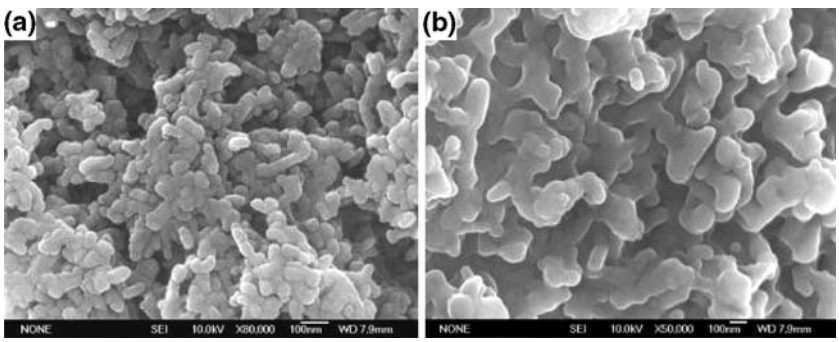

Fig. 1 SEM morphologies of the WT composite powders calcined at 800 °C (**a**) and 1050 °C (**b**)

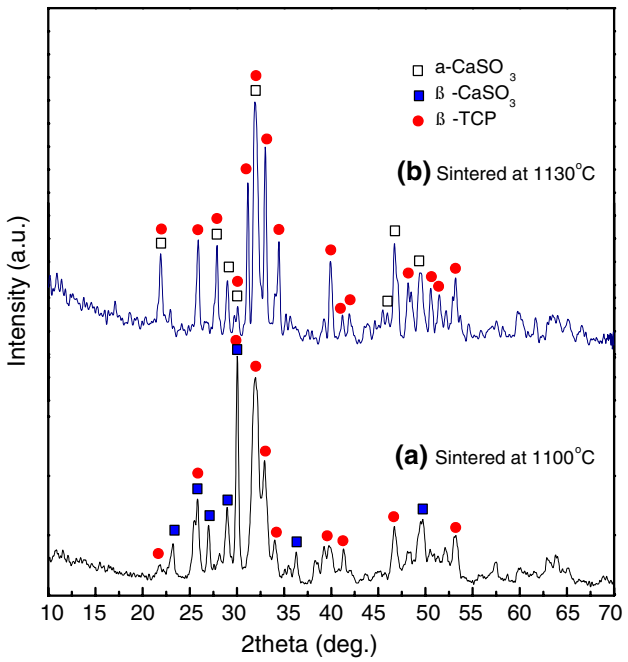

Fig. 3 X-ray diffraction patterns of the WT nano-sintered scaffolds at different temperatures

(SPS) [9]. This difference in the α-$CaSiO_3$ transition point could be due to the substantial temperature difference of SPS. Generally, the temperature of SPS is monitored with an optical pyrometer focused on a non-through hole of the graphite die, and there is some temperature difference between the measured and actual temperature which sometime rises to 200–250 °C [16]. Table 1 shows the mechanical properties of the WT nano-sintered scaffolds at different temperatures. The compressive strength and elastic modulus of the 1130 °C sintered WT scaffolds with the same porosity showed significant decrease when compared with those of the scaffolds sintered at 1100 °C. This difference was mainly ascribed to the formation of the hard brittle α-$CaSiO_3$ phase at higher temperature. The goal of achieving good mechanical properties in WT scaffolds is to avoid forming the α-$CaSiO_3$ phase during the sintering process.

The SEM micrograph of the nano-sintered WT scaffolds at 1100 °C is exhibited in Fig. 4a showing the macroporous structure. The shapes and sizes of the pores are similar to those of the PEG particulates. The macropore size is about 100–300 μm. The porosity is about 50% and the pore distribution is uniform to some extent. The SEM micrograph of the submicron-sintered scaffolds with the same porosity is shown in Fig. 4b. The macropores are quite similar to the nano-sintered scaffolds, which have a size ranging from 100 μm to 300 μm. The macropores created by porogens had an average shrinkage of 15–20% in size after sintering, which were due to the different shrinkage effect of the sintering compacts. The size of the original PEG particulates is in the range of 150–350 μm. It is acknowledged that [17] a minimum pore size of 100 μm is necessary for the porous scaffolds to function well, and pore sizes greater than 200 μm are essential requirements for osteoconduction. Thus, the pore size in the WT composites meets the requirements for bone graft scaffolds. The structure is favorable for bone tissue ingrowth. Higher magnification SEM pictures of the porous solid wall in Fig. 4c and d revealed that there existed some micro-interconnections with a size of 20–50 μm (indicated by the arrows) in the scaffolds. The interconnections are the pathways between the pores. They conduct cells and vessels between pores, favor osteoconduction, and bone ingrowth inside bioceramics. These connections could enable the circulation of body fluids for the supply of nutrients and the metabolic waste removal [18].

Table 1 Mechanical properties of the WT nano-sintered scaffolds at different temperatures

Sintering temperature (°C)	Porosity (%)	Compressive strength (MPa)	Elastic modulus (MPa)
1100	50 ± 1.0	16.2 ± 3.0	350 ± 30
1130	50 ± 1.0	8.3 ± 1.5	112 ± 15
1100	60 ± 1.0	6.43 ± 1.5	127 ± 25
1130	60 ± 1.0	5.12 ± 1.0	68 ± 20

The macropore walls of the nano-sintered and submicron-sintered scaffolds are dissimilar in their surface structure; the nano-sintered scaffolds are smooth, but the submicron-sintered counterparts are rough (Fig. 4c, d). For a clearer observation, the solid wall morphologies were examined, as shown in Fig 4e and f. The nano-sintered scaffolds showed much higher density and finer grain size than the submicron-sintered ones. The grain size is calculated from a high magnification SEM micrograph using mean linear intercept method. The mean grain size of the nano-sintered scaffolds is about 200 nm in the range of ''ultrafine'', while that of the micro scaffolds is about 2.0 μm in fine-grained range. There were some micropores in the macroporous walls. The micropores of the nano-sintered and submicron-sintered scaffolds are around 100 nm and 400 nm, respectively. The micropores could allow body fluid circulation whereas the macropores may provide a scaffold for bone-cell colonization. Although the micropores are not beneficial to the bone tissue ingrowth, they have significant effects on the degradation rate. The high densification rate resulting from the surface/interface effects of nanocomposite powders lead to a higher density of the scaffolds evidenced by smaller micropores and lower microporosity. In conclusion, the surface dissimilarity is a result of finer microstructures and higher density of the nano-sintered scaffolds.

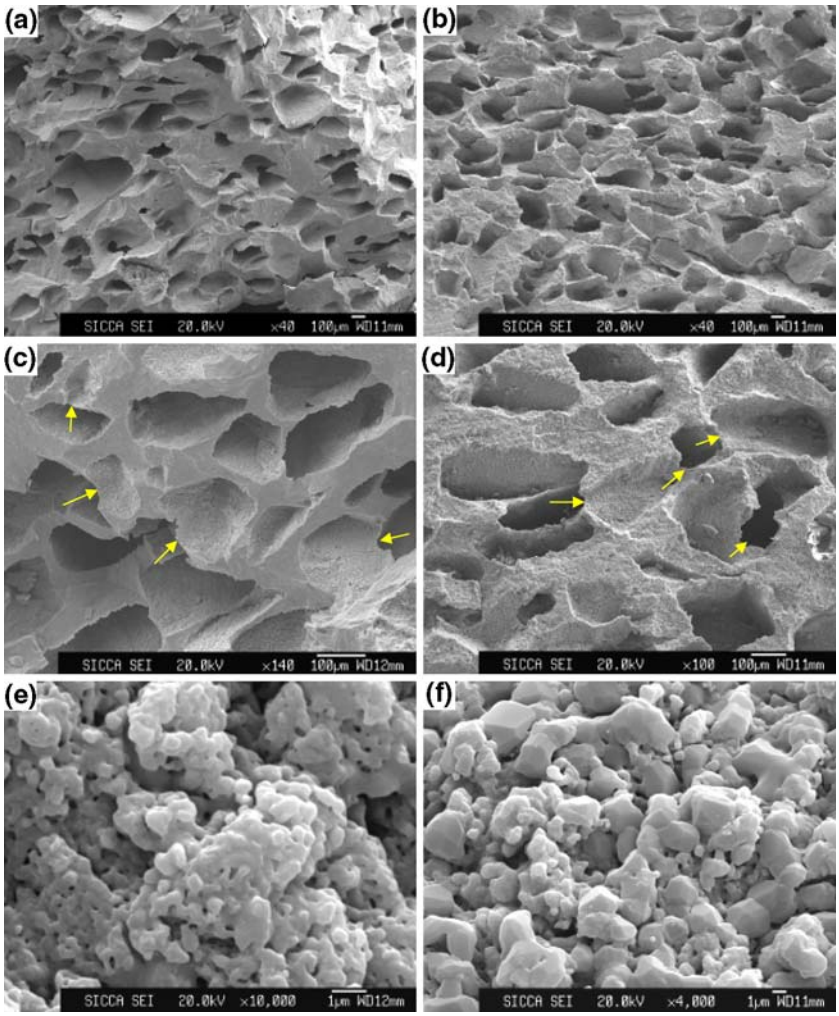

Fig. 4 SEM micrographs of the WT nano-sintered (**a**, **c**, **e**) and submicron-sintered scaffolds (**b**, **d**, **f**) showing the macroporous structure and macropore wall

The optimized microstructure in the nano-sintered scaffolds could result in mechanical property enhancement. Figure 5 illustrates the mechanical properties variation of the WT scaffolds as a function of porosity. Both the compressive strength and elastic modulus of the composites decreased as the porosity increased. Expectedly, the WT nano-sintered scaffolds exhibited much higher mechanical properties than their submicron-sintered counterparts (Fig. 5). The compressive strength and elastic modulus of the nano-sintered scaffolds with 50 ± 1.0% porosity are 16.2 ± 3.0 MPa and 350 ± 30 MPa, respectively. In contrast, the compressive strength of the submicron-sintered scaffolds is only 8.4 ± 2.0 MPa and the elastic modulus is only 180 ± 35 MPa. There was almost a twofold increase in mechanical properties for the nano-sintered scaffolds with porosity from 50 ± 1.0% to 65 ± 1.0%. The nano-sintered scaffolds provide excellent mechanical properties as predicted.

After goodness of fit test, it is found that the relationship between the porosity and strength behavior of the WT porous scaffolds obeys third-order exponential decay equation, as shown in Fig. 5. Rice [19] has proposed a function on the relationship of porosity with strength of ceramics,

$$\sigma = \sigma_0 \exp(-cp) \tag{3}$$

where σ_0 is zero-porosity strength, σ is the strength at pore volume fraction p, and the constant c is related directly to the pore characteristics such as pore shape and size. In this experiment, we used the same PEG porogen additions; therefore, σ_0 and c can be considered as constant. According to the above function, the strength (σ) should decrease exponentially as the pore volume fraction (p) increases. Our results in Fig. 5 are well in accordance with the above function. In this study, WT scaffolds were

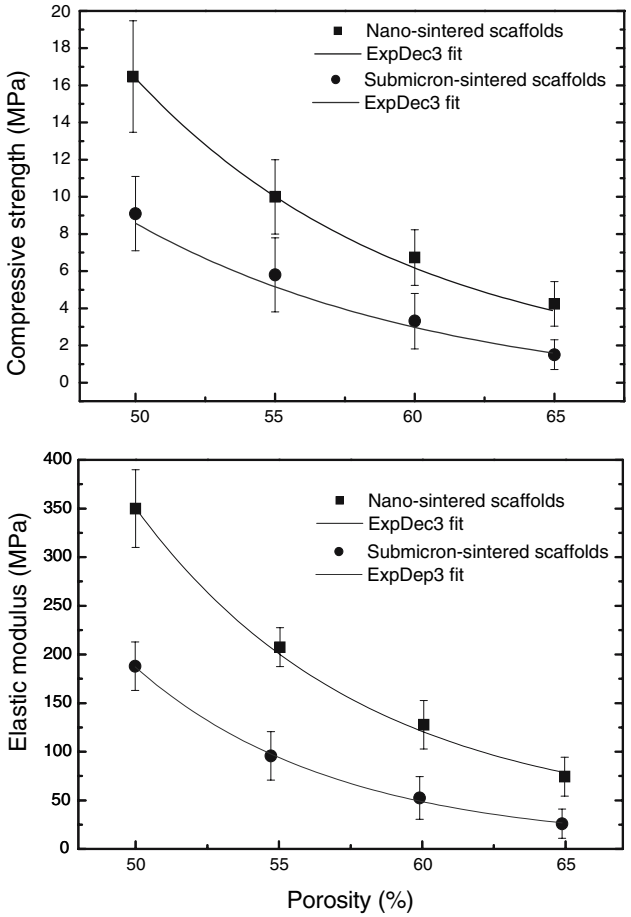

Fig. 5 Variation of compressive strength and elastic modulus as a function of porosity in WT scaffolds

fabricated from nanocomposite powders to balance the confliction between materials porosity and mechanical strength. Although the grain size of the WT scaffolds is only 200 nm in ultrafine grain range, experimental results showed that a substantial increase in mechanical properties over the submicron-sintered counterparts (grain size 2 μm) was achieved. The nano/nano composites strengthening mechanism in the dense nanocrystalline materials were also effective for porous bioceramics scaffolds.

Degradation in vitro

Figure 6 shows the variation of degradation of the nano-sintered and submicron-sintered WT composite scaffolds in Tris–HCl buffer solution. The degradation amount increased incrementally as a function of soaking time. The degradability value of the nano-sintered scaffolds with about 50% porosity reached 0.35% after 3 days soaking. As time increased, the degradation increased slowly to 4.5% at day 14 and finally to 5.0% by day 21. On the contrary, the degradation of the submicron-sintered scaffolds with 50%

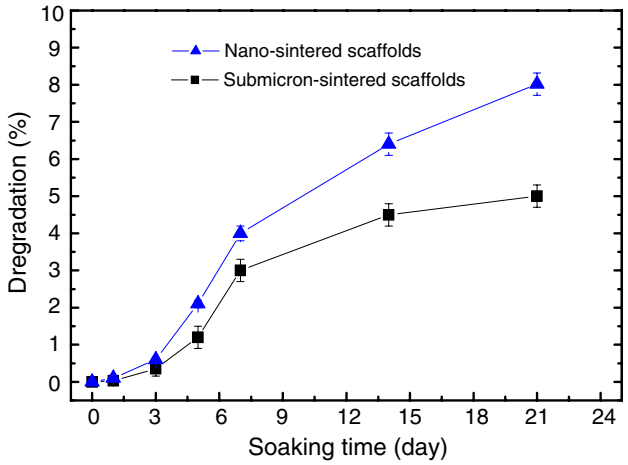

Fig. 6 Variation of the degradation of the WT scaffolds with soaking time

porosity was much faster than that of the nano-sintered ones. It reached 0.59% and 8.02% at day 3 and 21, respectively. The degradation rate for the submicron-sintered scaffolds was decreased faster over time when compared to that of the nano-sintered ones. The degradability of WT porous scaffolds plays a key role in its application as a bone graft material. The results in Fig. 6 showed that the degradation rate of the WT composite porous scaffolds could also be regulated by the grain size of bioceramics.

The degradation rate of Ca–P bioceramics is determined by sintering parameters, microstructure, porosity and crystallinity of the ceramics [20]. The porosity plays a dominant role in the degradation of bioceramics. The in-vivo study [21] has already confirmed that the degradation rate of the sintered bioceramics increased with the porosity increment due to the larger specific surface area. The degradation mechanism of the Ca–P bioceramics with good crystallization is mainly driven by dissolution and the dissolution occurs easily at the boundary of the micropores [22]. The nano-sintered WT scaffolds remain much smaller micropores and have lower microporosity than those of the submicron-sintered scaffolds with the same porosity. Thus, the specific surface area of pores in the nano-sintered scaffolds is lower than that of the submicron-sintered ones, which results in a decreased degradation rate.

After weight loss measurements, the compressive mechanical properties of the porous scaffolds were also measured in a dry state to evaluate the effects of degradation on the mechanical properties. Figure 7 shows the effect of the degradation on the mechanical properties of the scaffolds. In the first week, both the nano-sintered scaffolds and submicron-sintered ones showed little decrease in compressive strength. After soaking for 2 weeks in SBF, the compressive strength of nano-sintered scaffolds dropped about 11.7% from 16.2 MPa to 14.3 MPa, and that of the

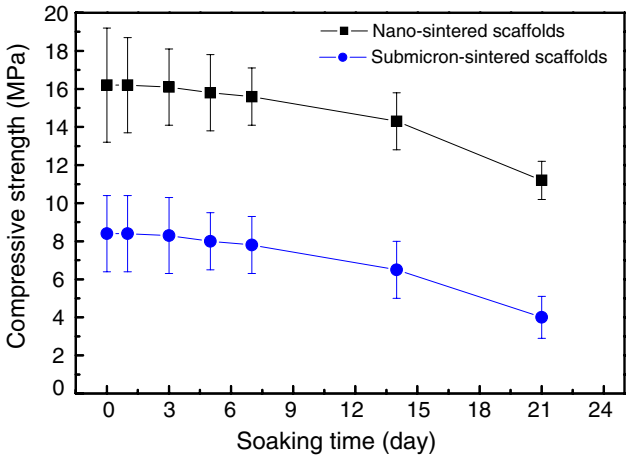

Fig. 7 Effect of degradation on the mechanical properties of the WT scaffolds

submicron-sintered scaffolds decreased about 20.7% from 8.2 MPa to 6.5 MPa. The strength of nano-sintered scaffolds was reduced 30.3% to 11.3 MPa and that of the submicron-sintered ones were reduced 50% to 4.1 MPa after being soaked for 3 weeks. The nano-sintered scaffolds showed less strength loss than their submicron-sintered counterparts did. This is due to the less weight loss and higher density of the nano-sintered scaffolds. The understanding of mechanical properties of WT scaffolds during degradation process is helpful for effective prediction of the degradation process; this will enable design of better implants for particular clinical applications. Above all, this comparative study on nano-sintered and submicron-sintered scaffolds prepared by the same method indicated that the macroporous WT nano-sintered scaffolds possessed excellent mechanical properties and regulated degradability. However, the pore forming method of the WT scaffolds should be adjusted to obtain higher porosity, better pore distribution, and enhanced interconnection for use as bone tissue engineering scaffolds. The present study has shown that the WT macroporous nano-sintered scaffolds have great potential as scaffolds for bone reconstruction applications.

Conclusions

WT macroporous nano-sintered scaffolds were successfully fabricated by using chemical precipitation and porogen burnout technique. The fabricated scaffolds showed porosity between 50 ± 1.0% and 65 ± 1.0% with a variety of macropores ranging from 100 μm to 300 μm in size. The WT nano-sintered scaffolds exhibited improved compressive strength and elastic modulus, about twice as high as the submicron-sintered scaffolds. The lower porous specific surface area of nano-sintered scaffolds was due to their lower degradation rate. The degradability of bioceramics scaffolds could be adjusted by manipulating the grain size of bioceramics. The nano-sintered scaffolds showed less strength loss than the submicron-sintered scaffolds during the degradation process. The WT macroporous nano-sintered scaffolds have great potential for application in bone reconstruction.

Acknowledgements The authors are grateful for the financial supports of the Science & Technology Commission of Shanghai Municipality of China (Project No. 0352nm119, No.05DJ14005), State 973 Program of China (Project No. 2005CB522704), Shanghai Postdoctoral Scientific Key Program (Project No. 06R214201), and China Postdoctoral Science Foundation (No. 20060390648). We would like to thank Mr. Lyndon F. Charles Jr. for his revision of the manuscript.

References

1. P. R. ANIL KUMAR, H. K. VARMA and T. V. KUMARY, *Acta Biomater.* **1** (2005) 545
2. L. L. HENCH, *J. Am. Ceram. Soc.* **81** (1998) 1705
3. M. KOHRI, K. MIKI, D. E. WAITE, H. NAKAJIMA and T. OKABE, *Biomaterials* **14** (1993) 299
4. J. M. BOULER, M. TRECANT, J. DELECRIN, J. ROYER, N. PASSUTI and G. DACULSIY, *J. Biomed. Mater. Res.* **32** (1996) 603
5. H. R. R. RAMAY and M. ZHANG, *Biomaterials* **25** (2004) 5171
6. P. N. DE AZA, F. GUITIAN and S. DE AZA, *Scripta Metall. Mater.* **31** (1994) 1001
7. P. SIRIPHANNONA, Y. KAMESHIMAA, A. YASUMORIA, K. OKADAA and S. HAYASHIB, *J. Eur. Ceram. Soc.* **22** (2002) 511
8. L. H. LONG, L. D. CHEN, S. Q. BAI, J. CHANG and K. L. LIN, *J. Eur. Ceram. Soc.* **26** (2006) 1701
9. L. H. LONG, L. D. CHEN and J. CHANG, *Ceram. Int.* **32** (2006) 457
10. S. NI, J. CHANG and L. CHOU, *J. Biomed. Mater. Res.* **76A** (2006) 196
11. K. L. LIN, J. CHANG, Y. ZENG and W. J. QIAN, *Mater. Lett.* **58** (2004) 2109
12. P. N. DE AZA, F. GUITIAN and S. DE AZA, *Biomaterials* **18** (1997) 1285
13. X. HUANG, D. L. JIANG and S. H. TAN, *J. Biomed. Mater. Res.* **69B** (2004) 70
14. Y. ZHANG and M. ZHANG, *J. Biomed. Mater. Res.* **61** (2002) 1
15. L. LE GUÉHENNEC, P. LAYROLLE and G. DACULSI, *Eur. Cells Mater.* **8** (2004) 3
16. F. ZHANG, J. SHEN and J. SUN, *Mater. Sci. Eng.* **381A** (2004) 86
17. D. M. LIU, *Ceram. Int.* **23** (1997) 135
18. J. X. LU, B. FLAUTRE, K. ANSELME, P. HARDOUIN, A. GALLUR, M. DESCAMPS and B. THIERRY, *J. Mater. Sci.: Mater. Med.* **10** (1999) 111
19. R. W. RICE, *J. Mat. Sci.* **28** (1993) 2187
20. J. X. LU, M. DESCAMPS, J. DEJOU, G. KOUBI, P. HARDOUIN, J. LEMAITRE and J. P. PROUST, *J. Biomed. Mater. Res.* **63** (2002) 408
21. C. P. A. T. KLEIN, A. A. DRIESSEN and K. DE GROOT, *J. Biomed. Mater. Res.* **17** (1983) 769
22. H. K. KOERTEN and J. VAN DER MEULEN, *J. Biomed. Mater. Res.* **44** (1999) 78